H1 restricts euchromatin-associated methylation pathways from heterochromatic encroachment

C. Jake Harris[1,2,5,#], Zhenhui Zhong[1,5], Lucia Ichino[1], Suhua Feng[1,3], Steven E. Jacobsen[1,3,4,#]

[1] Department of Molecular, Cell and Developmental Biology, University of California, Los Angeles, CA, USA.

[2] Present address: Department of Plant Sciences, University of Cambridge, Cambridge CB2 3EA, UK.

[3] Eli & Edythe Broad Center of Regenerative Medicine & Stem Cell Research, University of California, Los Angeles, Los Angeles, CA, USA.

[4] Howard Hughes Medical Institute, University of California, Los Angeles, CA, USA.

[5] These authors contributed equally.

[#] Correspondence: cjh92@cam.ac.uk and jacobsen@ucla.edu

ABSTRACT:

Silencing pathways prevent transposable element (TE) proliferation and help to maintain genome integrity through cell division. Silenced genomic regions can be classified as either euchromatic or heterochromatic, and are targeted by genetically separable epigenetic pathways. In plants, the RNA-directed DNA methylation (RdDM) pathway targets mostly euchromatic regions, while CMT methyltransferases are mainly associated with heterochromatin. However, many epigenetic features - including DNA methylation patterning - are largely indistinguishable between these regions, so how the functional separation is maintained is unclear. The linker histone H1 is preferentially localized to heterochromatin and has been proposed to restrict RdDM from encroachment. To test this hypothesis, we followed RdDM genomic localization in an *h1* mutant by performing ChIP-seq on the largest subunit, NRPE1, of the central RdDM polymerase (Pol V). Loss of H1 resulted in heterochromatic TE enrichment by NRPE1. Increased NRPE1 binding was associated with increased chromatin accessibility in *h1*, suggesting that H1 restricts NRPE1 occupancy by compacting chromatin. However, RdDM occupancy did not impact H1 localization, demonstrating that H1 hierarchically restricts RdDM positioning. H1 mutants experience major symmetric (CG and CHG) DNA methylation gains, and by generating an *h1/nrpe1* double mutant, we demonstrate these gains are largely independent of RdDM. However, loss of NRPE1 occupancy from a subset of euchromatic regions in *h1* corresponded to loss of methylation in all sequence contexts, while at ectopically bound heterochromatic loci, NRPE1 deposition correlated with increased methylation specifically in the CHH context. Additionally, we found that H1 restricts the occupancy of the methylation reader and activator complex component, SUVH1, indicating that H1's regulatory control of methylation pathways is not limited to RdDM. Together, the results support a model whereby H1 helps maintain the exclusivity of heterochromatin by preventing encroachment from other competing pathways.

INTRODUCTION:

Eukaryotic genomes are compartmentalized into euchromatic and heterochromatin regions (Ruiz-Velasco and Zaugg, 2017). In euchromatin, nucleosomes are more accessible, while in heterochromatin nucleosomes are more compacted and restrictive to transcription. Protein coding genes are typically euchromatic, while non-coding and repetitive elements more often reside in heterochromatin. However, transposable elements, which are targeted for DNA methylation and silencing, are found in both euchromatic and heterochromatic regions of the genome (Bourque et al., 2018). The pathways responsible for deposition of methylation and silencing of TEs in these different regions are functionally and genetically distinct (Du et al., 2015).

In plants, euchromatic repetitive regions are targeted by the RNA-directed DNA methylation pathway (RdDM) (Erdmann and Picard, 2020), in which the concerted action of non-coding RNA polymerases and small RNAs direct the DNA methyltransferase, DRM2, to specific sites of the genome. Newly invading genetic elements are targeted by the 'non-canonical' RdDM pathway, and involve the action of Pol II derived small RNAs (Cuerda-Gil and Slotkin, 2016). Once established, the canonical RdDM pathway takes over, whereby small RNAs are generated by the plant-specific polymerase IV (Pol IV). In both cases, a second plant-specific polymerase, Pol V, is an essential downstream component. The recruitment of Pol V to chromatin is stabilized by interaction with the DNA methylation readers SUVH2 and SUVH9 (Johnson et al., 2014). However, methylation alone is not sufficient to explain Pol V occupancy, as Pol V is restricted to the edges of long TEs and euchromatic methylated regions, despite methylation levels being high in the bodies of long TEs and in heterochromatin (Zhong et al., 2012). Therefore, additional mechanisms must exist to regulate Pol V occupancy.

Heterochromatin is targeted for DNA methylation and silencing by CMT methyltransferases (Stroud et al., 2014; Zemach et al., 2013). CMT3 and CMT2 are responsible for CHG and CHH methylation maintenance, respectively, at these regions. The CMTs form an epigenetic feedback loop with the KYP family of H3K9me2 methyltransferases, thereby maintaining high levels of repression-associated non-CG methylation and H3K9me2 at heterochromatic regions of the genome (Du et al., 2014, 2012; Li et al., 2018). As both DNA methylation and H3K9me2 are known to recruit components of the RdDM pathway (Johnson et al., 2014; Law et al., 2013), it is unclear how these regions remain functionally separated from RdDM.

The linker histone H1 associates with nucleosomes to modulate chromatin accessibility and higher order structures (Saha and Dalal, 2021). H1 binds to linker DNA as it exits from the nucleosome dyad and reduces linker DNA flexibility (Bednar et al., 2017). In plants, H1 is preferentially associated with heterochromatin, where it contributes to chromatin compaction (Bourguet et al., 2021; Choi et al., 2020; Rutowicz et al., 2019). Genetic evidence suggest that the chromatin remodeler DDM1 displaces H1 at heterochromatic TEs to facilitate access of CMT methyltransferases (Zemach et al., 2013), however, recent biochemical data suggests that this effect is likely indirect, via DDM1s interaction with the heterochromatin associated histone variant, H2A.W (Osakabe et al., 2021).

77

78 Since H1 physically locks genomic DNA to the nucleosome and is preferentially associated with
79 heterochromatin, it is a promising candidate for preventing RdDM encroachment into these regions.
80 Recent evidence supports this hypothesis, with RdDM associated small RNAs becoming more
81 heterochromatically enriched in *h1* knockouts (Choi et al., 2021; Papareddy et al., 2020). Here we
82 directly test whether RdDM occupancy is affected by loss of H1, by taking advantage of an endogenous
83 Pol V antibody (which recognizes Pol V's largest subunit, NRPE1). We found that *h1* antagonizes
84 NRPE1 occupancy throughout the genome, particularly at heterochromatic regions, and that this effect
85 is not limited to RdDM as it similarly impacts localization of the more recently discovered methyl-reader
86 and activator complex (Harris et al., 2018).

87

88

RESULTS:

To understand how H1 affects RdDM occupancy, we performed chromatin immunoprecipitation followed by sequencing (ChIP-seq) with a native antibody against NRPE1 (the largest catalytic subunit of Pol V, previously validated (Liu et al., 2018)). Two biological replicates of ChIP-seq in wild type control Col-0 and in *h1.1-1/h1.2-1* double mutant (hereafter referred to as WT and *h1,* respectively) were performed. As previously reported (Liu et al., 2018; Zhong et al., 2012), NRPE1 was enriched over short TEs and at the edges of long TEs in WT (Fig. 1A-B). In the *h1* mutant, however, NRPE1 enrichment was markedly increased, with NRPE1 invading the heterochromatic bodies of long TEs (Fig. 1A-B). The negative correlation between NRPE1 enrichment and TE length observed in WT was reverted in the *h1* mutant (Fig. 1C). This suggests that mutation of *h1* facilitates the invasion of NRPE1 to more heterochromatic regions, in which long TEs tend to reside. Consistent with this, NRPE1 increased more over heterochromatin associated CMT2 dependent hypo-CHH DMRs than at the RdDM associated DRM2 dependent CHH sites (Fig. 1D). The preferential enrichment of NRPE1 in *h1* was more pronounced at TEs that overlapped with heterochromatin associated mark, H3K9me2 (Fig. 1E). Comparing NRPE1 occupancy over TEs that had previously been classified by as either 'euchromatic' or 'heterochromatic' (based on a broad range of features and small RNA expression dynamics during embryonic development (Papareddy et al., 2020)), again, we found a striking increase in NRPE1 at heterochromatic over euchromatic TEs in *h1* (Fig. 1F). From a chromosomal viewpoint, NRPE1 was preferentially enriched over pericentromeric regions in *h1*, and showed corresponding depletion from the more euchromatic chromosomal arms (Fig. 1G, Supplementary Fig. 1). Importantly, we found no evidence for increased NRPE1 expression at the mRNA or protein level in the *h1* mutant (Supplementary Fig. 2). Together, the results indicate that H1 broadly restricts NRPE1 access to chromatin, and that this effect is more pronounced in heterochromatic regions of the genome. As H1 itself is preferentially localized to heterochromatin (see Fig. 1B,D,F) (Bourguet et al., 2021; Choi et al., 2020), this suggests that H1 directly antagonises RdDM occupancy.

One mechanism by which H1 could restrict RdDM access is by promoting chromatin compaction. Consistent with this idea and previous reports (Bourguet et al., 2021; Choi et al., 2020; He et al., 2019; Rutowicz et al., 2019), we observed increased accessibility in heterochromatic regions in *h1*, which mirrored the preferential recruitment of NRPE1 to heterochromatin (Supplementary Fig. 3AB). Loss of H1 mediated compaction in heterochromatin may be the indirect result of loss of heterochromatin associated marks such as H3K9me2. To examine this possibility, we performed H3K9me2 ChIP-seq, and although we observed some minor reductions in H3K9me2 in *h1*, the losses were not preferentially in heterochromatin where we see the majority of NRPE1 gain (Supplementary Fig. 3CD). This suggests that H1 primarily affects the accessibility, rather than the nature of chromatin at these heterochromatic regions.

To determine whether the antagonistic relationship between H1 and NRPE1 is reciprocal, we performed ChIP-seq using an endogenous antibody for H1, with two biological replicates in the WT and *nrpe1* mutant backgrounds. H1 levels were broadly unchanged in *nrpe1* at TE regions (Fig. 2A). Similarly,

129 over NRPE1 defined peaks (where NRPE1 occupancy is strongest in WT) we observed no change in
130 H1 occupancy in *nrpe1* (Fig. 2B). The results indicate that H1 does not invade RdDM regions in the
131 *nrpe1* mutant background.
132
133 Next, we asked whether ectopic recruitment of RdDM may be sufficient to evict H1 from the genome.
134 For this, we took advantage of the ZF-DMS3 transgenic lines that we previously characterized, in which
135 zinc finger (ZF) fused DMS3 can recruit endogenous NRPE1 to >10,000 ectopic sites throughout the
136 genome, corresponding to ZF 'off-target' binding sites (Gallego-bartolome et al., 2019). With these lines,
137 we performed NRPE1 and H1 ChIP-seq in parallel. Compared to the non-transgenic control, we
138 confirmed that NRPE1 was highly enriched at these 'off-target' regions (Fig 2C). However, with the
139 same material, we observed no depletion of H1 at the ectopically bound NRPE1 sites (Fig. 2C). To
140 exclude the possibility that NRPE1 alone may be insufficient to evict H1, but that the fully functioning
141 RdDM pathway may be required (which constitutes at least 32 described proteins acting in concert
142 (Matzke and Mosher, 2014)), we focused on the subset of ZF-DMS3 off-target sites that experience
143 hyper-CHH methylation (Gallego-bartolome et al., 2019). The gain of ectopic methylation at these
144 regions indicates that the full RdDM pathway is recruited and functions to deposit *de novo* methylation.
145 However, even at these regions where H1 is mildly enriched in WT, we saw no evidence for H1
146 depletion in the ZF-DMS3 transgenic lines (Fig. 2D). Together, these results indicate that H1
147 hierarchically and non-reciprocally restricts RdDM from overaccumulation in heterochromatin.
148
149 Given our observation that NRPE1 is redistributed in *h1*, we wondered whether this could help to explain
150 some of the unusual methylation defects observed in the *h1* mutant. For instance, *h1* mutants
151 experience contrasting loss and gain of DNA methylation at euchromatic and heterochromatic TEs,
152 respectively (Bourguet et al., 2021; Zemach et al., 2013). Previous explanations to account for this
153 suggested that the *h1* afforded increased accessibility of euchromatic TEs may promote increased
154 access by activation-associated chromatin modifying enzymes, which in turn antagonise DNA
155 methylation (Zemach et al., 2013). However, based on our NRPE1 ChIP-seq observations, we
156 hypothesized a simpler scenario, whereby the euchromatic loss and heterochromatic gain of
157 methylation is caused by the relative shift of RdDM from euchromatin to heterochromatin. To directly
158 test this possibility, we generated two independent NRPE1 CRISPR knockouts in the *h1* mutant
159 background (Supplementary Fig. 4AB), and performed whole genome bisulphite sequencing (WGBS)
160 analysis, alongside *nrpe1*, *h1* and WT controls. We confirmed *nrpe1* loss of function in the independent
161 CRISPR KO lines by plotting CHH methylation over NRPE1 associated high confidence DMRs (Zhang
162 et al., 2018), finding that CHH methylation is entirely abolished over these regions in both *nrpe1/h1*
163 lines (Supplementary Fig. 4C). By analysis of chromosome level DNA methylation patterns in the
164 different mutant backgrounds, we found that the striking pericentromeric increase in CG and CHG
165 methylation observed in *h1*, is almost entirely independent of RdDM, as it was not rescued in *nrpe1/h1*
166 (Fig. 3A, Supplementary Fig. 5). In contrast, CHH methylation was mostly unaltered between the
167 genotypes at the chromosome scale, with evidence for a slight reduction of CHH in the *h1/nrpe1* double
168 mutant as compared to *h1* alone (Fig. 3A, Supplementary Fig. 5).
169

170 Next, we compared methylation levels in euchromatic versus heterochromatic TEs. Heterochromatic
171 TEs experienced major increases in CG and CHG methylation in *h1* as previously reported (Zemach et
172 al., 2013), and these were independent of NRPE1 function, as the same increases were observed in
173 *nrpe1/h1* (Fig. 3B). CHH levels were largely unchanged at heterochromatic TEs in all mutant
174 backgrounds (Fig. 3B). At euchromatic TEs, CG and CHG methylation levels were largely unchanged
175 in *h1*, while CHH levels were markedly reduced as previously reported (Fig. 3C). CHH methylation
176 levels were further reduced in *nrpe1*, consistent with the well-established role of RdDM in maintaining
177 CHH at euchromatic TEs (Stroud et al., 2013), with the additional mutation of *h1* in *nrpe1/h1* having a
178 minimal effect (Fig. 3C). However, we noticed that the loss of CHG methylation in *nrpe1* was largely
179 rescued in the *nrpe1/h1* double mutant (Fig. 3C). This striking effect was specific to euchromatic TEs.
180 NRPE1 is therefore required for CHG methylation maintenance at euchromatic TEs and in the absence
181 of H1, loss of RdDM can be functionally compensated for by other methylation pathways. This
182 compensation is likely due to the action of CMT3 (Stroud et al., 2014; Zemach et al., 2013). The effect
183 is reminiscent of *h1*'s amelioration of methylation loss in the chromatin remodeler *ddm1* mutant
184 (Zemach et al., 2013), and further supports a role for H1 in demarcating the boundary between
185 heterochromatic and euchromatic methylation pathways.
186
187 Calling differentially methylated regions (DMRs) in the mutant backgrounds, we found that *h1* hyper
188 CHG DMRs were by far the most numerous as compared to any other context (Fig. 4A). Consistent
189 with the average methylation chromosomal and TE plots, these hyper CHG DMRs were highly enriched
190 over pericentromeric heterochromatin (Fig. 4B). To gain insight into the functional context of methylation
191 in these regions, we performed overlap analysis between *h1* hyper CHG DMRs and DMRs from 96
192 other Arabidopsis gene silencing mutants that were published previously (Stroud et al., 2013). Building
193 similarity matrices based on pairwise overlapping scores (Co-Occurrence Statistics), we observed
194 separation of clustering of mutants belonging to different functional pathways (Fig. 4C, Supplementary
195 Fig. 6), consistent with previous studies (Stroud et al., 2013; Zhang et al., 2018). The *h1* hyper CHG
196 DMRs clustered primarily with components of the CG maintenance pathway, including *met1* and
197 *vim1/2/3* (Fig. 4D). Interestingly, the *h1* hyper CHG DMRs also clustered and correlated strongly with
198 *ddm1* hyper CHH DMRs. As heterochromatic transposons are known to transition from a state of
199 quiescence to being actively targeted by RdDM in the *ddm1* mutant (Panda et al., 2016), this again
200 suggests that H1 controls regions of the genome that are susceptible to spurious RdDM targeting.
201
202 While the majority of methylation changes observed in *h1* (hyper CG and CHG) were entirely
203 independent of NRPE1, in the chromosomal plots we noted a subtle depletion of CHH methylation in
204 the *h1/nrpe1* double mutant as compared to *h1* alone (Fig. 3A), suggesting that redistribution of NRPE1
205 may have functional consequences on methylation patterning. To explicitly investigate these ectopically
206 bound loci, we compared NRPE1 enrichment in WT versus *h1* and identified 15,075 peaks that have
207 significantly higher NRPE1 signal in the *h1* mutant. At these regions, CG and CHG methylation changes
208 broadly mirrored that of heterochromatic TEs, again supporting the notion that NRPE1 primarily
209 redistributes to heterochromatic regions of the genome in *h1* (Fig. 5A, Supplementary Fig. 7A).

210 However, we also observed a significant depletion of CHH methylation at these regions in the *nrpe1/h1*
211 double mutant, as compared to either the *h1* and *nrpe1* alone, which was not observed when looking
212 at heterochromatic TEs as a whole (compare Fig. 5A to Fig. 3B). This indicates that NRPE1 facilitates
213 active deposition of CHH methylation at these newly bound locations. Reciprocally, we asked how
214 methylation changes at regions of the genome that lose NRPE1 in *h1* (1,859 peaks), and we found that
215 methylation levels are significantly depleted in all three contexts (CG, CHG and CHH) in the *h1*, *nrpe1*
216 and *nrpe1/h1* double mutant backgrounds (Fig. 5B, Supplementary Fig. 7B and 8). The mirrored loss
217 and gain of methylation with changes in NRPE1 occupancy indicates that NRPE1 redistribution in *h1*
218 directly impacts methylation patterning *in cis*.
219
220 The results thus far support a model whereby H1 prevents RdDM encroachment into heterochromatin.
221 As H1 likely restricts access by reducing chromatin accessibility at these regions, we reasoned that this
222 effect would not be RdDM specific and could affect other machinery in a similar manner. Recently we
223 identified a transcriptional activator complex, consisting of SUVH1, SUVH3, DNAJ1 and DNAJ2 (Harris
224 et al., 2018). The SUVH1/3 methyl binding proteins directly bind CHH methylation *in vitro*, yet *in vivo*
225 the complex shows strong preferential recruitment to RdDM sites, but not to CMT2 deposited CHH
226 heterochromatic sites (Harris et al., 2018). We therefore wondered whether complex's occupancy might
227 also be affected by H1. To test this, we performed ChIP-seq on SUVH1-3xFLAG in an *h1* mutant
228 background (Fig. 6A). As with NRPE1, SUVH1 increased in the *h1* background significantly more in
229 heterochromatin, with preferential enrichment over long TEs, *cmt2* dependent hypo CHH DMRs, and
230 heterochromatic TEs (Fig. 6B). Therefore, the effect of H1 is not RdDM specific, and acts to demarcate
231 the boundary between euchromatic and heterochromatic methylation pathways, likely through
232 promoting nucleosome compaction and restricting heterochromatin access.

233 **DISCUSSION:**

234 Here we show that loss of H1 results in redistribution of RdDM from euchromatic to heterochromatic
235 regions, consistent with recent findings from small RNA data (Choi et al., 2021; Papareddy et al., 2020).
236 This antagonism, however, appears non-reciprocal, as H1 levels were not affected by RdDM loss, or
237 artificial gain at ectopic regions of the genome. H1-mediated restriction could be in part due to its
238 structural capacity to reduce linker DNA flexibility (Bednar et al., 2017), thereby reducing polymerase
239 access to unwind and interact with genomic DNA. Pol V requires the DDR complex for efficient
240 association with chromatin (Wongpalee et al., 2019), so the presence of H1 could present an additional
241 barrier to this complex. Given that H1 has been shown to compact chromatin in part through the phase
242 separating property of its highly charged intrinsically disordered domain (Gibson et al., 2019), another
243 possibility is that high H1 occupancy creates a biophysical environment that excludes Pol V and related
244 complexes. Our data together with the observed heterochromatic encroachment of Pol IV dependent
245 small RNAs in *h1* (Choi et al., 2021; Papareddy et al., 2020), along with H1's recently described role in
246 preventing spurious antisense transcription at protein coding genes (Choi et al., 2020), support a
247 polymerase indiscriminate model for H1's antagonism.

248

249 Small RNAs are relatively abundant in heterochromatin, despite Pol IV and RdDM being dispensable
250 for methylation in these regions (Stroud et al., 2014). This suggests that Pol IV occupies
251 heterochromatin, but that RdDM is either impotent for methylation deposition or acts redundantly with
252 the CMT/KYP pathway. Here we detect NRPE1-dependent methylation at heterochromatic loci in *h1,*
253 and combined with the finding that Pol V does not appreciably enter these regions in WT, suggests that
254 H1 prevents RdDM from fully mobilizing in these regions by blocking Pol V. Recent evidence suggests
255 that Pol V can be directly recruited by small RNAs to establish methylation (Sigman et al., 2021), and
256 therefore mechanisms that preclude Pol V recruitment to heterochromatin would be particularly crucial
257 in preventing redundant RdDM activity at regions where methylation has already been established.

258

259 In *Arabidopsis thaliana*, RdDM targets evolutionarily young transposable elements (Zhong et al., 2012).
260 H1 therefore helps to improve the efficiency of RdDM by focusing it upon TEs with the greatest potential
261 to mobilize. As transposons age, they eventually become targeted by CMTs. How this transition occurs
262 is unclear, but our results indicate a potential role for progressive accumulation of H1 in this process.
263 Interestingly in tomato, CMTs rather than RdDM target the evolutionarily younger elements (Wang and
264 Baulcombe, 2020), therefore it will be important to determine whether H1 plays a similar role in
265 maintaining the barrier between methylation pathways in this context. Recent work has shown that H1
266 co-operates with H2A.W to promote compaction at heterochromatic regions (Bourguet et al., 2021).
267 However, H2A.W was found to antagonize rather than promote H1 deposition at heterochromatin.
268 Therefore, the features that drive H1 to preferentially incorporate into heterochromatin are yet to be
269 discovered.

METHODS:

Plant materials and growth conditions:

Arabidopsis thaliana plants in this study were Col-0 ecotype and were grown under 16h light: 8h dark condition (on soil), or under constant light (on plates). The following plant materials were used: wild-type (WT, non-transgenic), *h1* (double homozygous mutant consisting of, *h1.1-1* [SALK_128430] and *h1.2–1* [GABI_406H11], originally described by (Zemach et al., 2013)), *nrpe1* (*nrpe1-11* [SALK_029919]), DMS3-ZF (this is a homozygous transgenic line containing the pEG302-DMS3-3xFLAG-ZF construct in Col-0 WT, originally described by (Gallego-bartolome et al., 2019)), SUVH1-3xFLAG in *suvh1* (this is a complementing homozygous transgenic line containing the pEG302-gSUVH1-3xFLAG construct in *suvh1-1*, originally described by (Harris et al., 2018)), SUVH1-3xFLAG in *h1* (this line was generated for this work, by transforming the same pEG302-gSUVH1-3xFLAG construct into the *h1.1-1* [SALK_128430] and *h1.2–1* [GABI_406H11] double mutant background), and the *h1*/*nrpe1* CRISPR lines (described below).

Generation of CRISPR lines:

Two independent NRPE1 knockout lines were generated in the background of *h1* (*h1.1-1 h1.2-1* double, see above), designated as *h1/nrpe1* cKO_49 and *h1/nrpe1* cKO_63. The lines were generated using the previously published pYAO::hSpCas9 system (Yan et al., 2015) as described by (Ichino et al., 2021). Briefly, the two guides (ATTCTTGACGGAGAGATTGT, and TCTGGCACTGACAAACAGTT) targeting hSpCas9 to NRPE1 (AT2G40030) exons were sequentially cloned in the SpeI linearized pYAO::hSpCas9 construct by In-Fusion (Takara, cat #639650). The final vector was electroporated into AGL0 agrobacteria and transformed in *h1* mutant plants by agrobacterium-mediated floral dipping. T1 plants were selected on ½ MS agar plates with hygromycin B and were PCR genotyped to identify plants with deletions spanning the guide region. Selected lines were taken to T2 and genotyped to identify those that had segregated out the pYAO::hSpCas9 transgene. Cas9 negative plants that were homozygous for an NRPE1 deletion (*h1/nrpe1* cKO_49) or an indel-induced frameshift to premature stop codon (*h1/nrpe1* cKO_63) were confirmed in the T3 generation (see Supplementary Fig. 4).

Chromatin immunoprecipitation (ChIP) and western blot:

All the material for ChIP used in this paper were from pooled 10-12 days old seedlings grown on Murashinge and Skoog agar plates (1/2X MS, 1.5% agar, pH5.7). The ChIP protocol used has been previously described (Ichino et al., 2021; Villar and Kohler, 2018), with minor modifications. Briefly, 2-4g of seedling tissue was used for each sample. Samples were ground in liquid nitrogen and crosslinked for 10 or 12 minutes at room temperature in Nuclei Isolation buffer (50mM Hepes pH8, 1M sucrose, 5mM KCl, 5mM MgCl2, 0.6% triton X-100, 0.4mM PMSF, 5mM benzamidine hydrochloride, cOmplete EDTA-free Protease Inhibitor Cocktail (Roche)) containing 1% formaldehyde. The crosslinking reactions were stopped with 125mM glycine by incubation at room temperature for 10 minutes. Crosslinked nuclei were filtered through one layer of miracloth, washed with Extraction Buffer 2, centrifuged through a layer of Extraction Buffer 3 and lysed with Nuclei lysis buffer (buffer compositions are described in the published protocol (Villar and Kohler, 2018)). Chromatin was sheared using a

310 Bioruptor Plus (Diagenode) (20 cycles of 30 seconds on and 30 seconds off) and immunoprecipitated
311 overnight at 4°C with antibody. anti-NRPE1 (endogenous antibody, described in (Liu et al., 2018)), anti-
312 H1 (Agrisera, AS11 1801), anti-H3K9me2 (abcam, 1220), anti-H3 (abcam, 1791), anti-FLAG (for both
313 the SUVH1-3xFLAG and the DMS3-ZF ChIPs, we used Anti-FLAG M2 (Sigma, F1804)). 25µl each of
314 Protein A and Protein G magnetic Dynabeads (Invitrogen) were added to each sample and incubated
315 for 2 more hours at 4°C. The immunoprecipitated chromatin was washed with Low Salt (2X), High Salt,
316 LiCl and TE buffers, for 5 minutes each at 4°C (buffer compositions are described in the published
317 protocol (Villar and Kohler, 2018)) and eluted twice with 250µl of elution buffer (1% SDS and 0.1M
318 NaHCO3) in a thermomixer at 65°C and 1000 rpm, 20 minutes for each elution. Reverse crosslinking
319 was performed overnight at 65°C in 0.2M NaCl, and proteins were degraded by proteinase K treatment
320 at 45°C for 5h. The DNA fragments were purified using phenol:chloroform and ethanol precipitated
321 overnight at -20°C. Libraries were prepared using the Ovation Ultralow System V2 kit (NuGEN,
322 0344NB-A01) following the manufacturer's instructions, with 15 cycles of PCR. Libraries were
323 sequenced on a HiSeq 4000 or NovaSeq 6000 instrument (Illumina) using either single- or paired-end
324 50bp reads.
325
326 For the western blot shown in Supplementary Fig. 2B, 100ul of sheared chromatin was used as the
327 input material for SDS-PAGE (as previously described (Harris et al., 2016)), using the anti-NRPE1 and
328 anti-H1 antibodies described above.
329
330 **ChIP-seq data analysis:**
331 ChIP-seq data were aligned to the TAIR10 reference genome with Bowtie2 (v2.1.0) (Langmead and
332 Salzberg, 2012) allowing only uniquely mapping reads with zero mismatch. Duplicated reads were
333 removed by Samtools. ChIP-seq peaks were called by MACS2 (v2.1.1) and annotated with ChIPseeker
334 (Yu et al., 2015). Differential peaks were called by bdgdiff function in MACS2 (Zhang et al., 2008). ChIP-
335 seq data metaplots were plotted by deeptools (v2.5.1) (Ramírez et al., 2016).
336
337 **Whole-genome bisulfite sequencing (BS-seq) library preparation:**
338 Whole genome bisulfite sequencing libraries were generated as previously described (Harris et al.,
339 2016), with minor modifications. The DNeasy Plant Mini Kit (Qiagen #69104) was used to isolate
340 genomic DNA. 150µg of genomic DNA was used as input, a Covais S2 instrument was used for
341 shearing (2 minutes), the Epitect Kit (QIAGEN #59104) was used for bisulfite conversion, and the
342 Ultralow Methyl Kit (NuGEN) was used for library preparation and paired-end libraries were sequenced
343 on a NovaSeq 6000 instrument.
344
345 **Whole-genome bisulfite sequencing (BS-seq) data analysis:**
346 Previously published whole-genome bisulfite sequencing data for mutants and wild type were
347 reanalyzed from previous paper (Stroud et al., 2013). Briefly, Trim_galore
348 (http://www.bioinformatics.babraham.ac.uk/projects/trim_galore/) was used to trim adapters. BS-seq
349 reads were aligned to TAIR10 reference genome by BSMAP (v2.90) and allowed 2 mismatches and 1

350 best hit (-v 2 -w 1) (Xi and Li, 2009). Reads with three or more consecutive CHH sites were considered
351 as unconverted reads and filtered. DNA methylation levels were defined as #C/ (#C + #T). DMR
352 overlapping analysis were conducted by mergePeaks (-d 100) of Homer (Heinz et al., 2010) with WGBS
353 data published previously (Stroud et al., 2013). The estimated conversion rates for all WGBS libraries
354 are provided in Supplementary Table 1.
355
356 **Data and code availability:**
357 Data supporting the findings of this work are available within the paper and its Supplementary
358 Information files. All high-throughput sequencing data generated in this study are accessible at NCBI's
359 Gene Expression Omnibus (GEO) via GEO Series accession number GSE225480
360 (https://www.ncbi.nlm.nih.gov/geo/query/acc.cgi?acc=GSE225480). The customized codes used in this
361 study are available upon reasonable request. The following secure token has been created to allow
362 review of record GSE225480 while it remains in private status: XXX
363
364 **ACKNOWLEDGEMENTS:**
365 We thank Suhua Feng and Mahnaz Akhavan for support with high-throughput sequencing at the UCLA
366 Broad Stem Cell Research Center BioSequencing Core Facility. C.J.H is supported by a Royal Society
367 University Research Fellowship (URF\R1\201016). This work was supported by NIH R35 GM130272
368 to S.E.J.. S.E.J is an Investigator of the Howard Hughes Medical Institute.
369
370 **AUTHOR CONTRIBUTIONS:**
371 C.J.H. and S.E.J. designed the research. C.J.H., Z.Z. and S.E.J. wrote the manuscript. L.I. helped to
372 isolate the *h1/nrpe1* CRISPR knockout lines. S.F. generated the WGBS libraries from genomic DNA.
373 C.J.H. performed all other experiments. Z.Z. and C.J.H. performed the bioinformatic analyses.
374
375

REFERENCES:

Bednar J, Garcia-Saez I, Boopathi R, Cutter AR, Papai G, Reymer A, Syed SH, Lone IN, Tonchev O, Crucifix C, Menoni H, Papin C, Skoufias DA, Kurumizaka H, Lavery R, Hamiche A, Hayes JJ, Schultz P, Angelov D, Petosa C, Dimitrov S. 2017. Structure and Dynamics of a 197 bp Nucleosome in Complex with Linker Histone H1. *Mol Cell* **66**:384-397.e8. doi:10.1016/j.molcel.2017.04.012

Bourguet P, Picard CL, Yelagandula R, Pélissier T, Lorković ZJ, Feng S, Pouch-Pélissier MN, Schmücker A, Jacobsen SE, Berger F, Mathieu O. 2021. The histone variant H2A.W and linker histone H1 co-regulate heterochromatin accessibility and DNA methylation. *Nat Commun* **12**:1–12. doi:10.1038/s41467-021-22993-5

Bourque G, Burns KH, Gehring M, Gorbunova V, Seluanov A, Hammell M, Imbeault M, Izsvák Z, Levin HL, Macfarlan TS, Mager DL, Feschotte C. 2018. Ten things you should know about transposable elements 06 Biological Sciences 0604 Genetics. *Genome Biol* **19**:1–12. doi:10.1186/s13059-018-1577-z

Choi J, Lyons DB, Kim MY, Moore JD, Zilberman D. 2020. DNA Methylation and Histone H1 Jointly Repress Transposable Elements and Aberrant Intragenic Transcripts. *Mol Cell* **77**:310-323.e7. doi:10.1016/j.molcel.2019.10.011

Choi J, Lyons DB, Zilberman D. 2021. Histone H1 prevents non-cg methylation-mediated small RNA biogenesis in arabidopsis heterochromatin. *Elife* **10**:1–24. doi:10.7554/eLife.72676

Cuerda-Gil D, Slotkin RK. 2016. Non-canonical RNA-directed DNA methylation. *Nat Plants* **2**. doi:10.1038/nplants.2016.163

Du J, Johnson LM, Groth M, Feng S, Hale CJ, Li S, Vashisht A a., Gallego-Bartolome J, Wohlschlegel J a., Patel DJ, Jacobsen SE. 2014. Mechanism of DNA methylation-directed histone methylation by KRYPTONITE. *Mol Cell* **55**:495–504. doi:10.1016/j.molcel.2014.06.009

Du J, Johnson LM, Jacobsen SE, Patel DJ. 2015. DNA methylation pathways and their crosstalk with histone methylation. *Nat Rev Mol Cell Biol* **16**:519–532. doi:10.1038/nrm4043

Du J, Zhong X, Bernatavichute Y V, Stroud H, Feng S, Caro E, Vashisht A a, Terragni J, Chin HG, Tu A, Hetzel J, Wohlschlegel J a, Pradhan S, Patel DJ, Jacobsen SE. 2012. Dual binding of chromomethylase domains to H3K9me2-containing nucleosomes directs DNA methylation in plants. *Cell* **151**:167–80. doi:10.1016/j.cell.2012.07.034

Erdmann RM, Picard CL. 2020. RNA-directed DNA Methylation, PLoS Genetics. doi:10.1371/journal.pgen.1009034

Gallego-bartolome J, Liu W, Kuo PH, Feng S, Ghoshal B, Gardiner J, Park SY, Chory J, Jacobsen SE, Liu W, Kuo PH, Feng S, Ghoshal B, Gardiner J, Zhao JM, Park SY, Chory J, Jacobsen SE. 2019. Co-targeting RNA Polymerases IV and V Promotes and V Promotes Efficient De Novo DNA Methylation in Arabidopsis. *Cell* **176**:1–15. doi:10.1016/j.cell.2019.01.029

Gibson BA, Doolittle LK, Schneider MWG, Jensen LE, Gamarra N, Henry L, Gerlich DW, Redding S, Rosen MK. 2019. Organization of Chromatin by Intrinsic and Regulated Phase Separation. *Cell* **179**:470-484.e21. doi:10.1016/j.cell.2019.08.037

Harris CJ, Husmann D, Liu W, Kasmi F El, Wang H, Papikian A, Pastor WA, Moissiard G, Vashisht AA,

416 Dangl JL, Wohlschlegel JA, Jacobsen SE. 2016. Arabidopsis AtMORC4 and AtMORC7 Form
417 Nuclear Bodies and Repress a Large Number of Protein-Coding Genes. *PLOS Genet*
418 **12**:e1005998. doi:10.1371/journal.pgen.1005998
419 Harris CJ, Scheibe M, Wongpalee SP, Liu W, Zhong Z, Yen L, Barshop WD, Rayatpisheh S, Du J,
420 Rothbart SB, Butter F, Jacobsen SE. 2018. A DNA methylation reader complex that enhances
421 gene transcription. *Science* **362**:1182–1186.
422 He S, Vickers M, Zhang J, Feng X. 2019. Natural depletion of histone H1 in sex cells causes DNA
423 demethylation, heterochromatin decondensation and transposon activation. *Elife* **8**:1–23.
424 doi:10.7554/ELIFE.42530
425 Heinz S, Benner C, Spann N, Bertolino E, Lin YC, Laslo P, Cheng JX, Murre C, Singh H, Glass CK.
426 2010. Simple Combinations of Lineage-Determining Transcription Factors Prime cis-Regulatory
427 Elements Required for Macrophage and B Cell Identities. *Mol Cell* **38**:576–589.
428 doi:10.1016/j.molcel.2010.05.004
429 Ichino L, Boone BA, Strauskulage L, Harris CJ, Kaur G, Gladstone MA, Tan M, Feng S, Jami-alahmadi
430 Y, Duttke SH. 2021. MBD5 and MBD6 couple DNA methylation to gene silencing through the J-
431 domain protein SILENZIO. *Science (80-)* **1439**:1434–1439.
432 Johnson LM, Du J, Hale CJ, Bischof S, Feng S, Chodavarapu RK, Zhong X, Marson G, Pellegrini M,
433 Segal DJ, Patel DJ, Jacobsen SE. 2014. SRA- and SET-domain-containing proteins link RNA
434 polymerase V occupancy to DNA methylation. *Nature* **507**:124–128. doi:10.1038/nature12931
435 Langmead B, Salzberg SL. 2012. Fast gapped-read alignment with Bowtie 2. *Nat Methods* **9**:357–359.
436 doi:10.1038/nmeth.1923
437 Law J a, Du J, Hale CJ, Feng S, Krajewski K, Palanca AMS, Strahl BD, Patel DJ, Jacobsen SE. 2013.
438 Polymerase IV occupancy at RNA-directed DNA methylation sites requires SHH1. *Nature*
439 **498**:385–389. doi:10.1038/nature12178
440 Li X, Harris CJ, Zhong Z, Chen W, Liu R, Jia B, Wang Z, Li S, Jacobsen SE, Du J. 2018. Mechanistic
441 insights into plant SUVH family H3K9 methyltransferases and their binding to context-biased non-
442 CG DNA methylation. *PNAS* 1–10. doi:10.1073/pnas.1809841115
443 Liu W, Duttke SH, Hetzel J, Groth M, Feng S, Gallego-Bartolome J, Zhong Z, Kuo HY, Wang Z, Zhai J,
444 Chory J, Jacobsen SE. 2018. RNA-directed DNA methylation involves co-transcriptional small-
445 RNA-guided slicing of polymerase v transcripts in Arabidopsis. *Nat Plants* **4**:181–188.
446 doi:10.1038/s41477-017-0100-y
447 Matzke M a., Mosher R a. 2014. RNA-directed DNA methylation: an epigenetic pathway of increasing
448 complexity. *Nat Rev Genet* **15**:394–408. doi:10.1038/nrg3683
449 Naish M, Alonge M, Wlodzimierz P, Tock AJ, Abramson BW, Schmücker A, Mandáková T, Jamge B,
450 Lambing C, Kuo P, Yelina N, Hartwick N, Colt K, Smith LM, Ton J, Kakutani T, Martienssen RA,
451 Schneeberger K, Lysak MA, Berger F, Bousios A, Michael TP, Schatz MC, Henderson IR. 2021.
452 The genetic and epigenetic landscape of the Arabidopsis centromeres. *Science (80-)* **374**.
453 doi:10.1126/science.abi7489
454 Osakabe A, Jamge B, Axelsson E, Montgomery SA, Akimcheva S, Kuehn AL, Pisupati R, Lorković ZJ,
455 Yelagandula R, Kakutani T, Berger F. 2021. The chromatin remodeler DDM1 prevents transposon

456 mobility through deposition of histone variant H2A.W. *Nat Cell Biol* **23**:391–400.
457 doi:10.1038/s41556-021-00658-1
458 Panda K, Ji L, Neumann DA, Daron J, Schmitz RJ, Slotkin RK. 2016. Full-length autonomous
459 transposable elements are preferentially targeted by expression-dependent forms of RNA-
460 directed DNA methylation. *Genome Biol* **17**:170. doi:10.1186/s13059-016-1032-y
461 Papareddy RK, Páldi K, Paulraj S, Kao P, Lutzmayer S, Nodine MD. 2020. Chromatin regulates
462 expression of small RNAs to help maintain transposon methylome homeostasis in Arabidopsis.
463 *Genome Biol* **21**:251. doi:10.1186/s13059-020-02163-4
464 Ramírez F, Ryan DP, Grüning B, Bhardwaj V, Kilpert F, Richter AS, Heyne S, Dündar F, Manke T.
465 2016. deepTools2: a next generation web server for deep-sequencing data analysis. *Nucleic Acids*
466 *Res* **44**:W160–W165. doi:10.1093/nar/gkw257
467 Ruiz-Velasco M, Zaugg JB. 2017. Structure meets function: How chromatin organisation conveys
468 functionality. *Curr Opin Syst Biol* **1**:129–136. doi:10.1016/j.coisb.2017.01.003
469 Rutowicz K, Lirski M, Mermaz B, Teano G, Schubert J, Mestiri I, Kroteń MA, Fabrice TN, Fritz S, Grob
470 S, Ringli C, Cherkezyan L, Barneche F, Jerzmanowski A, Baroux C. 2019. Linker histones are
471 fine-scale chromatin architects modulating developmental decisions in Arabidopsis. *Genome Biol*
472 **20**:1–22. doi:10.1186/s13059-019-1767-3
473 Saha A, Dalal Y. 2021. A glitch in the snitch: The role of linker histone H1 in shaping the epigenome in
474 normal and diseased cells. *Open Biol* **11**. doi:10.1098/rsob.210124
475 Sigman MJ, Panda K, Kirchner R, McLain LL, Payne H, Peasari JR, Husbands AY, Slotkin RK, McCue
476 AD. 2021. An siRNA-guided ARGONAUTE protein directs RNA polymerase V to initiate DNA
477 methylation. *Nat Plants* **7**:1461–1474. doi:10.1038/s41477-021-01008-7
478 Stroud H, Do T, Du J, Zhong X, Feng S, Johnson L, Patel DJ, Jacobsen SE. 2014. Non-CG methylation
479 patterns shape the epigenetic landscape in Arabidopsis. *Nat Struct Mol Biol* **21**:64–72.
480 doi:10.1038/nsmb.2735
481 Stroud H, Greenberg MVC, Feng S, Bernatavichute Y V, Jacobsen SE. 2013. Comprehensive Analysis
482 of Silencing Mutants Reveals Complex Regulation of the Arabidopsis Methylome. *Cell* **152**:352–
483 364. doi:10.1016/j.cell.2012.10.054
484 Villar CBR, Kohler C. 2018. Plant Chromatin immunoprecipitation. *Methods Mol Biol* **1839**:65–75.
485 doi:10.1007/978-1-4939-8685-9_7
486 Wang Z, Baulcombe DC. 2020. Transposon age and non-CG methylation. *Nat Commun* **11**:1–9.
487 doi:10.1038/s41467-020-14995-6
488 Wongpalee SP, Liu S, Gallego-Bartolomé J, Leitner A, Aebersold R, Liu W, Yen L, Nohales MA, Kuo
489 PH, Vashisht AA, Wohlschlegel JA, Feng S, Kay SA, Zhou ZH, Jacobsen SE. 2019. CryoEM
490 structures of Arabidopsis DDR complexes involved in RNA-directed DNA methylation. *Nat*
491 *Commun* **10**:1–12. doi:10.1038/s41467-019-11759-9
492 Xi Y, Li W. 2009. BSMAP: Whole genome bisulfite sequence MAPping program. *BMC Bioinformatics*
493 **10**:1–9. doi:10.1186/1471-2105-10-232
494 Yan L, Wei S, Wu Y, Hu R, Li H, Yang W, Xie Q. 2015. High-Efficiency Genome Editing in Arabidopsis
495 Using YAO Promoter-Driven CRISPR/Cas9 System. *Mol Plant* **8**:1820–1823.

496 doi:10.1016/j.molp.2015.10.004
497 Yu G, Wang LG, He QY. 2015. ChIP seeker: An R/Bioconductor package for ChIP peak annotation,
498 comparison and visualization. *Bioinformatics* **31**:2382–2383. doi:10.1093/bioinformatics/btv145
499 Zemach A, Kim MY, Hsieh P-H, Coleman-Derr D, Eshed-Williams L, Thao K, Harmer SL, Zilberman D.
500 2013. The Arabidopsis nucleosome remodeler DDM1 allows DNA methyltransferases to access
501 H1-containing heterochromatin. *Cell* **153**:193–205. doi:10.1016/j.cell.2013.02.033
502 Zhang H, Zhang F, Yu Y, Feng L, Jia J, Liu B, Li B, Guo H, Zhai J. 2020. A Comprehensive Online
503 Database for Exploring ~20,000 Public Arabidopsis RNA-Seq Libraries. *Mol Plant* **13**:1231–1233.
504 doi:10.1016/j.molp.2020.08.001
505 Zhang Y, Harris CJ, Liu Q, Liu W, Ausin I, Long Y, Xiao L, Feng L, Chen Xu, Xie Y, Chen Xinyuan,
506 Zhan L, Feng S, Li JJ, Wang H, Zhai J, Jacobsen SE. 2018. Large-scale comparative epigenomics
507 reveals hierarchical regulation of non-CG methylation in Arabidopsis. *Proc Natl Acad Sci*
508 201716300. doi:10.1073/pnas.1716300115
509 Zhang Y, Liu T, Meyer CA, Eeckhoute J, Johnson DS, Bernstein BE, Nussbaum C, Myers RM, Brown
510 M, Li W, Shirley XS. 2008. Model-based analysis of ChIP-Seq (MACS). *Genome Biol* **9**.
511 doi:10.1186/gb-2008-9-9-r137
512 Zhong X, Hale CJ, Law JA, Johnson LM, Feng S, Tu A, Jacobsen SE. 2012. DDR complex facilitates
513 global association of RNA polymerase V to promoters and evolutionarily young transposons. *Nat*
514 *Struct Mol Biol* **19**:870–5. doi:10.1038/nsmb.2354
515

FIGURES:

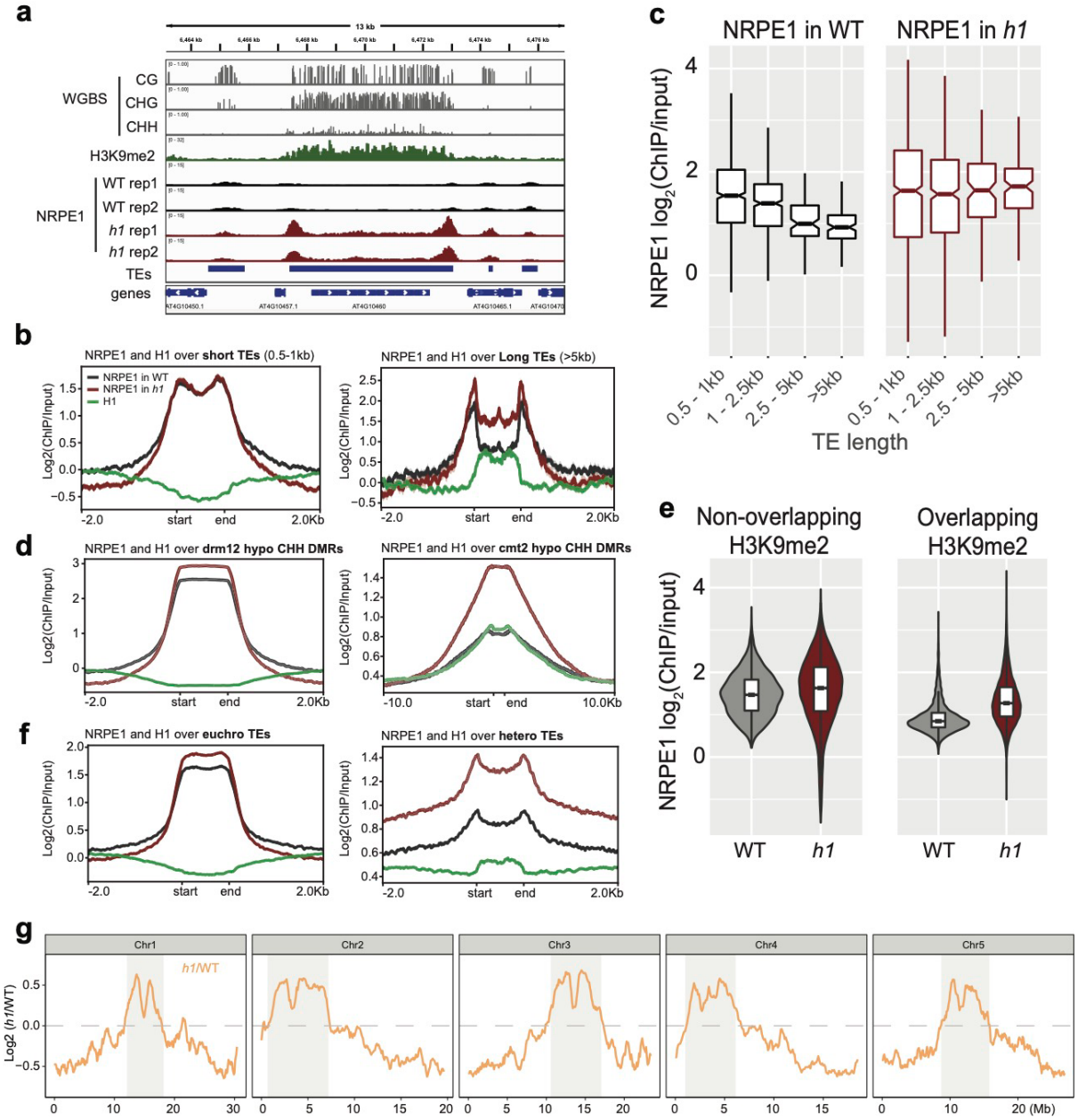

Figure 1 - NRPE1 accumulates in heterochromatin in an *h1* mutant background: A) Genome browser image showing increased NRPE1 enrichment in *h1* over heterochromatic (long, H3K9me2 enriched) and not euchromatic (short, not H3K9me2 enriched) TEs. B) metaplot showing ChIP-seq enrichment of NRPE1 in WT vs. *h1*, and H1 occupancy in WT for reference (data from GSE122394), at short vs. long TEs. C) boxplot showing association between NRPE1 and TE length in WT and *h1*. D) As in B) for *drm12* vs. *cmt2* hypo CHH DMRs. E) Violin plot inlaid with boxplot showing enrichment of NRPE1 at TEs that overlap with H3K9me2 peaks, vs. TEs that do not, in WT vs. *h1*. F) as in B) at euchromatic vs. heterochromatic TEs. G) Chromosomal plots showing NRPE1 enrichment in *h1* as compared to WT, with pericentromeric regions denoted in grey.

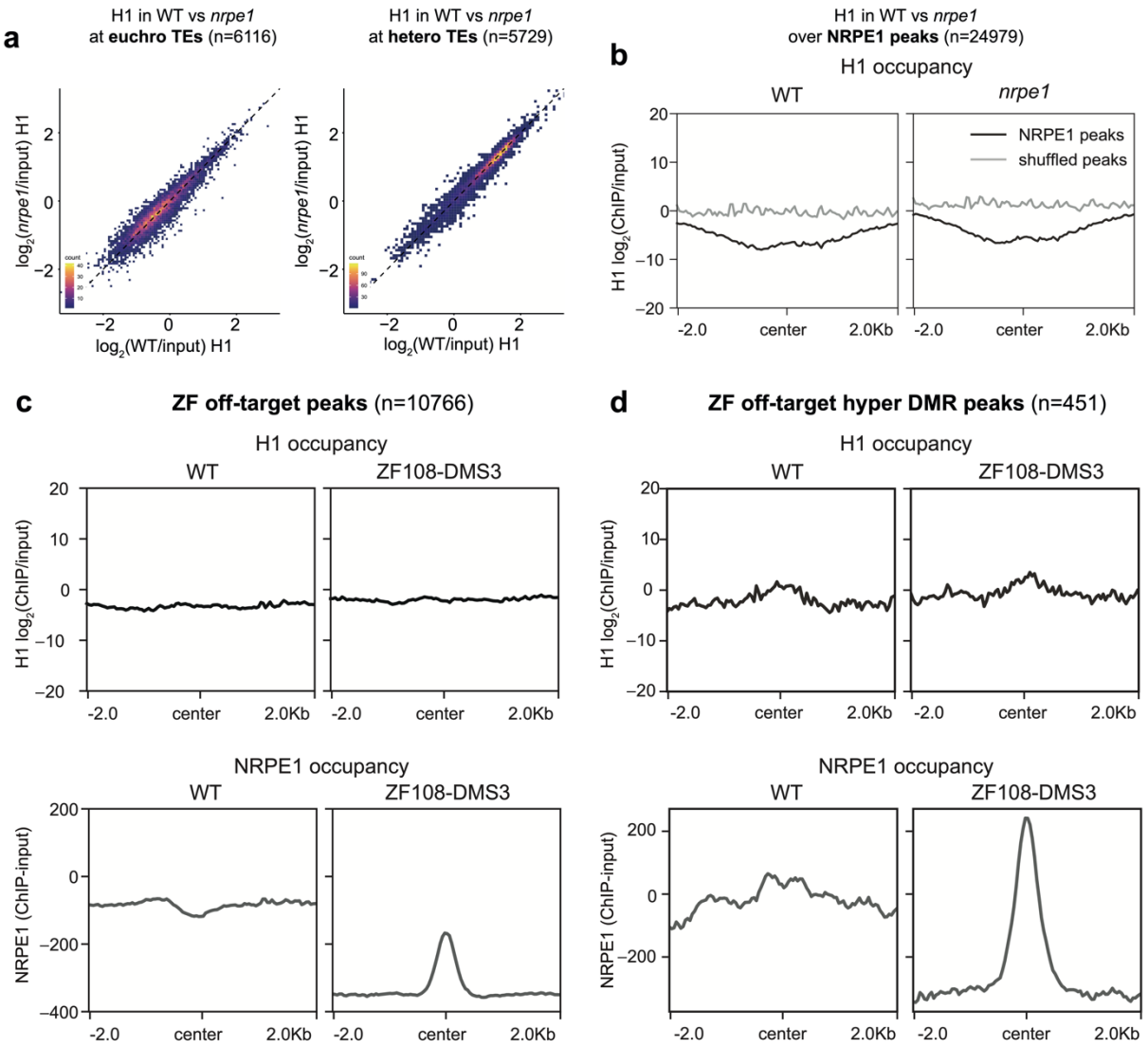

Figure 2 - RdDM does not reciprocally affect H1 localization: A) Scatter plot showing H1 enrichment in WT vs. *nrpe1* at euchromatic vs heterochromatic TEs. B) Metaplot showing H1 enrichment at NRPE1 peaks in WT vs. *nrpe1* C) H1 and NRPE1 occupancy at ZF-DMS3 off target peaks. Upper panel: H1 occupancy in WT vs. ZF108-DMS3. Lower panel: NRPE1 occupancy in WT vs. ZF108-DMS3. Chromatin from the same sample was used for both H1 and NRPE1 ChIP-seq data, so the lower panel serves as a control showing that ZF108-DMS3 is recruited to these off-target regions in these samples, despite H1 localisation remaining unchanged. D) Same as C) at the subset of regions where CHH methylation is gained in ZF108-DMS3 (Liu et al 2018), indicating that the fully functioning RdDM pathway is recruited to these regions.

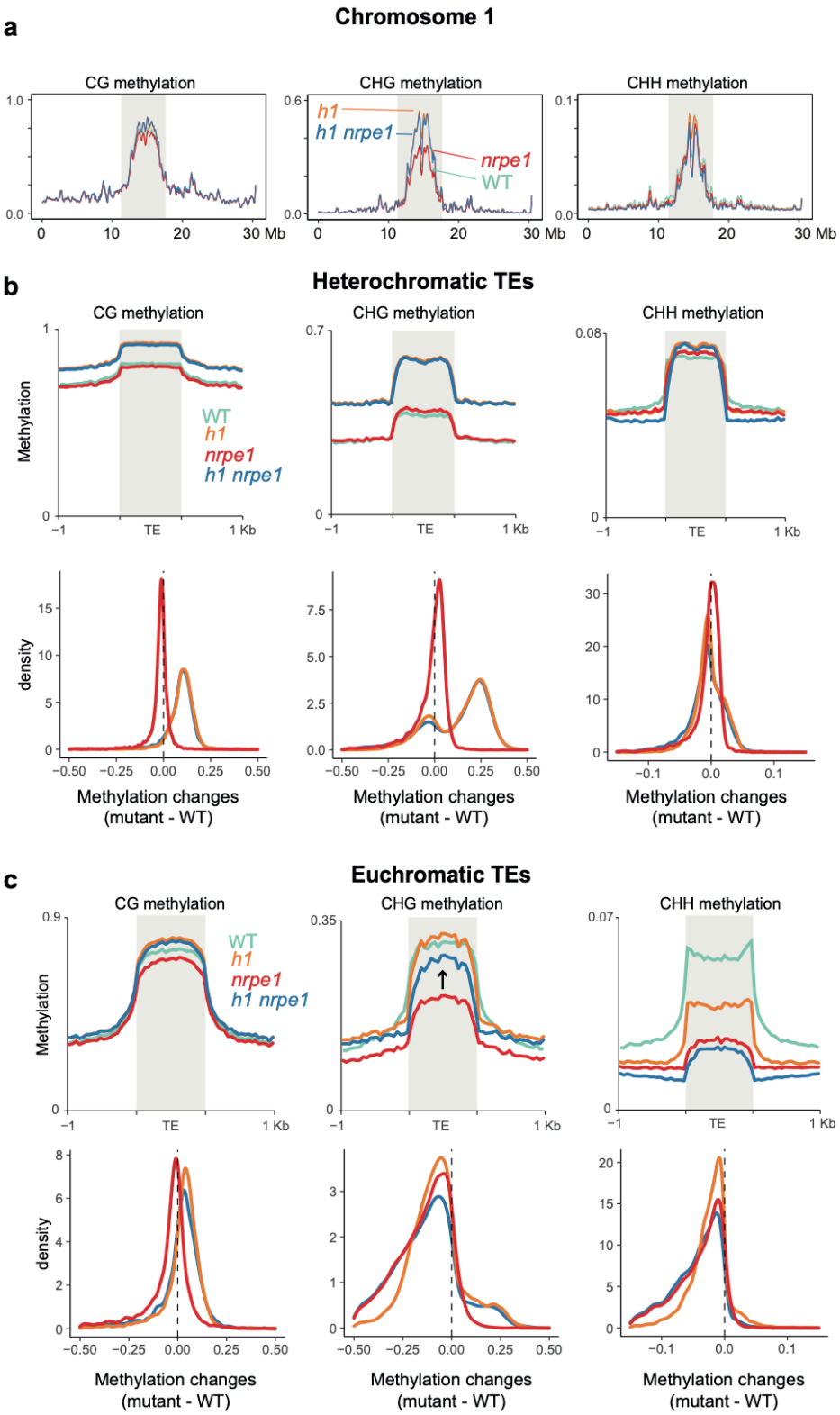

524

Figure 3 - Major CG and CHG methylation gains in *h1* are independent of RdDM: A) Chromosomal view of DNA methylation levels (average of 10kb windows) in the genotypes indicated on chromosome 1. Y-axis indicates fraction methylation (0-1). B) Methylation level over heterochromatic TEs. Upper panel: metaplots, Lower panel - kernel density plots. x-axis indicates change in methylation fraction mutant minus WT. C) Methylation level over euchromatic TEs. Upper panel: metaplots, Lower panel - kernel density plots. Arrow highlights the gain in CHG methylation in the *h1/nrpe1* double mutant, as compared to *nrpe1* alone.

525

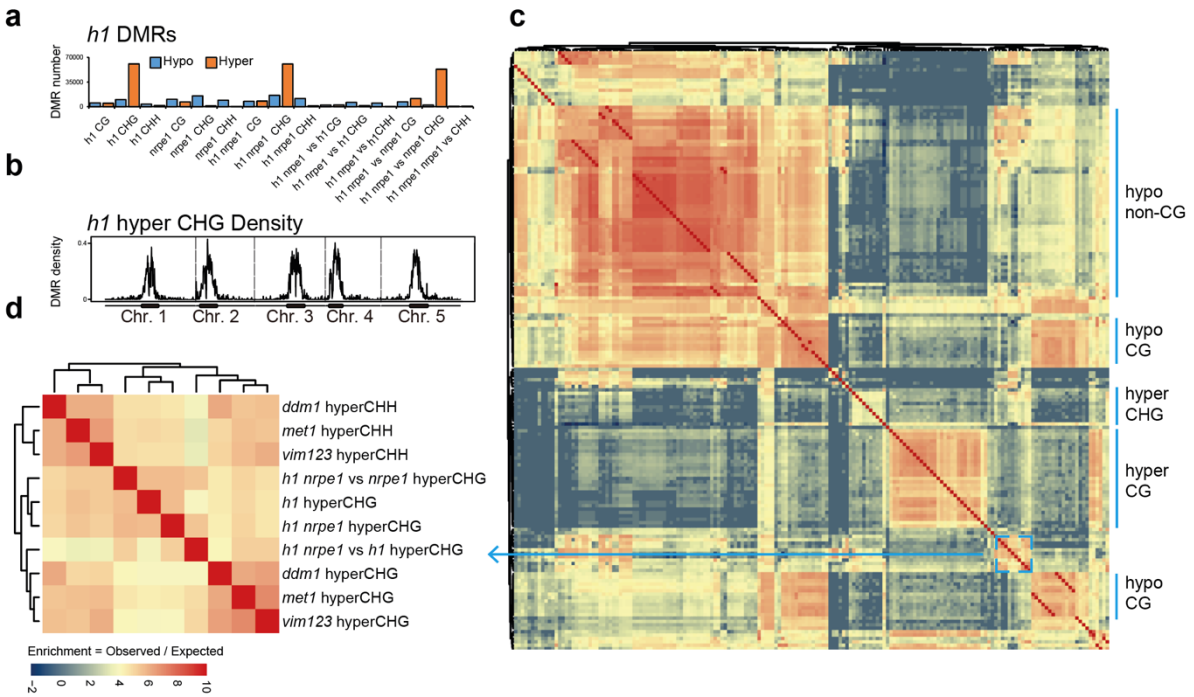

Figure 4 - Overlap analysis of *h1* hyper CHG DMRs with 96 methylation mutants: A) hypo vs hyper DMR number for the comparisons indicated. B) *h1* hyper CHG DMR density over chromosomes 1-5. C) heatmap showing pairwise comparisons of DMRs grouped by major methylation effects (individual genotypes are shown in Supplementary Figure 6). Colour scale represents observed / expected values. D) Zoomed in view of *h1* hyper CHG cluster shown C) (see blue box and arrow).

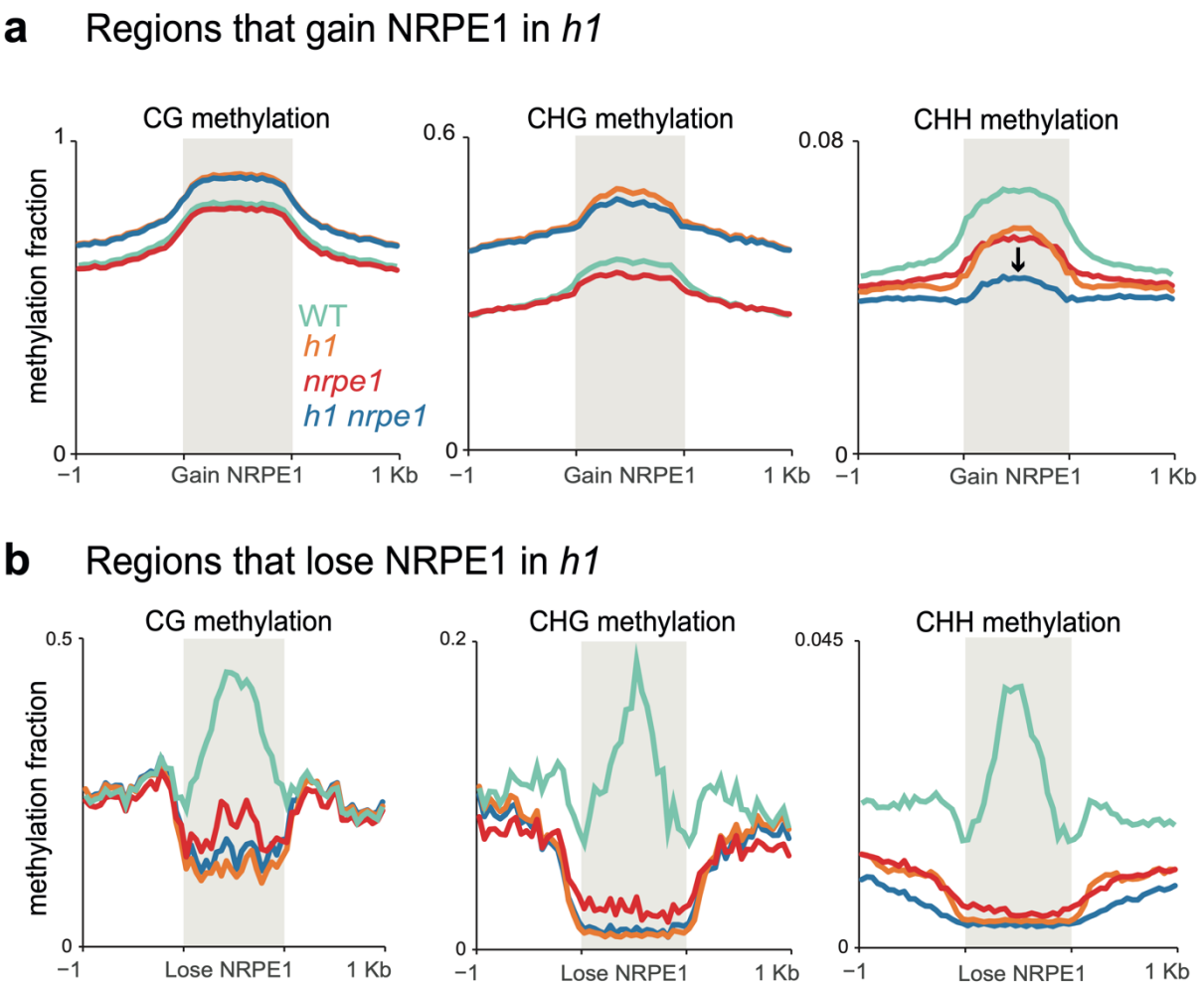

Figure 5 - Patterns of NRPE1 re-localisation in *h1* show corresponding methylation changes: A) Methylation metaplot in the genotypes indicated over regions of the genome that gain NRPE1 in *h1*. Arrow highlights the change in average CHH methylation in the *h1/nrpe1* double mutant as compared to the single mutants. B) Methylation metaplot of the genotypes indicated over regions of the genome that lose NRPE1 in *h1*.

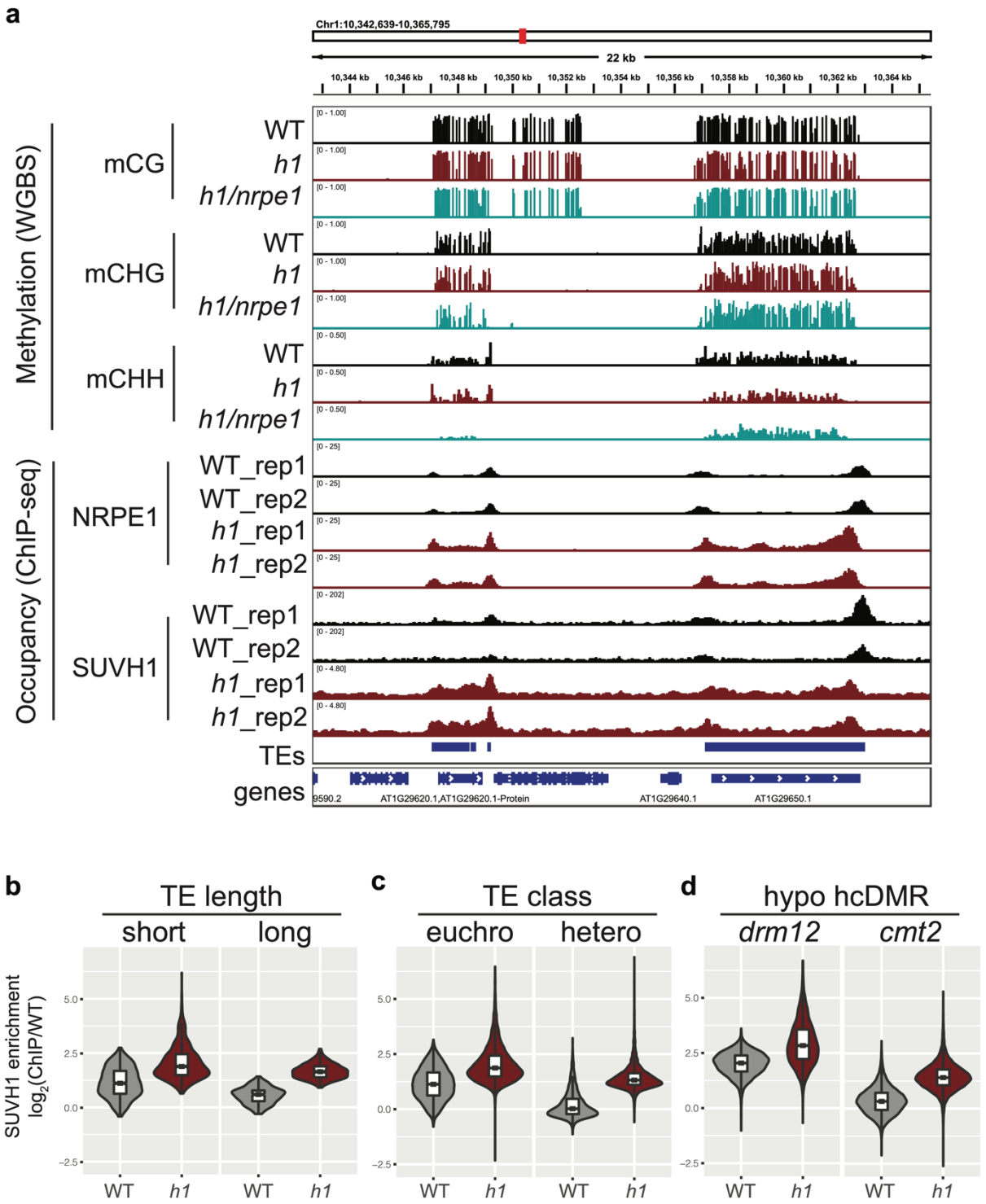

Figure 6 - SUVH1 encroaches heterochromatin in an *h1* mutant background: A) Genome browser image showing SUVH1 re-localisation in *h1* mirrors that of NRPE1. B-D) Boxplot inlaid violin plots showing SUVH1 enrichment in WT vs *h1* at short vs long TEs (B), at euchromatic vs heterochromatic TEs (C) and at drm12 vs cmt2 hypo CHH DMRs (D).